Quantum Entanglement Generation in Autonomous Thermal Machines: Effects of Non-Markovianity, Hilbert Space Structure, and Quantum Coherence

A. Khoudiri,^{1,*} K. El Anouz,^{1,†} and A. El Allati^{1,‡}

We present a theoretical investigation of entanglement generation in an external quantum system via interaction with a quantum autonomous thermal machine (QATM) under non-Markovian dynamics. The QATM, composed of two qubits each coupled to independent thermal reservoirs, interacts with an external system of two additional qubits. By analyzing the Hilbert space structure, energy level configurations, and temperature gradients, we define a common interaction between the QATM qubits and the external system qubits, which allows the definition of two thermodynamic cycles (A and B) governed by virtual temperatures and energy-conserving transitions. We demonstrate that the QATM can act as a structured reservoir capable of inducing non-Markovian memory effects, as highlighted by negative entropy production rates. Using mutual information and concurrence, we show that entanglement is generated only under cycle A, which is associated with stronger non-Markovian behavior and higher coherence correlations. Our results demonstrate that temperature differences, Hilbert space structure, and coherence serve as quantum resources for controlling and enhancing entanglement in quantum thermodynamic settings, with parameters consistent with experimental superconducting qubit platforms.

PACS numbers: 05.70.Ln, 05.30.-d 03.67.-a 42.50.Dv

I. INTRODUCTION

In the framework of quantum thermodynamics, quantum autonomous thermal machines (QATMs) are important viewpoints to link quantum thermodynamic theory to quantum thermodynamic technologies [1–3]. The role of QATMs has been discussed in different frameworks, such as boosting quantum batteries and measuring low temperatures as quantum thermometry [4, 5]. It also includes the effect on correlations in quantum many-body systems [6]. In another context, many papers discussed quantum entanglement generation via QATMs, including maximal steady-state entanglement generation [7–9]. The investigation of linear quantum thermal machines for entanglement generation at low temperatures shows entanglement production between environments [10].

The Hilbert space structure as a quantum resource in multilevel quantum thermal machines is provided in [11], where the relation between the Hilbert space dimension and the performance of the machines is discussed. It also includes the notion of virtual qubits and virtual temperature [12, 13] to investigate temperature reservoirs as quantum resources to ensure the autonomy of the machine, and the role of virtual temperature in their functioning [12, 13].

We present in our recent work [15] the dynamical effect of QATMs on the external system, and the capability of the QATM to produce the memory effect based on the exchange of correlations with the external sys-

tem. We also presented the relationship between non-Markovianity and the Landauer bound [16] in the context of the autonomous quantum thermal machine. Generally, we link quantum thermodynamics and quantum information theory in the framework of autonomous quantum thermal machines.

Through the contexts mentioned previously, we highlight in this paper the entanglement generation via autonomous quantum thermal machines, including an expansion of our work [15], linking the quantum thermodynamics framework with Hilbert space structure [16–18], non-Markovianity [19–22], virtual temperatures, and correlations in entanglement generation [23–26].

In our scenario, we investigate a quantum autonomous thermal machine (QATM) composed of two qubits [12, 15, each interacting with two bosonic reservoirs, hot and cold, respectively. A structured external system consisting of two additional qubits is coupled to the QATM qubits. We analyze the Hilbert space structure of the QATM and the external system qubits to design the interaction between them based on temperature and energy constraints [11]. Using the concepts of virtual temperature and virtual qubits of the QATM [13], together with the common interaction between the QATM and external system qubits, we define two thermodynamic cycles, denoted A and B, which allow us to investigate the effects of the reservoirs' temperature differences and the Hilbert space structure. Mathematically, we express the temperature transitions between cycles A and B as a function of the energy spacing of the QATM gubits. We numerically examine the validity of our theoretical framework for the thermodynamic cycles by analyzing the heat and temperature dynamics of each subsystem [27]. To ensure thermodynamic consistency, we also investigate the second law of quantum thermodynamics through entropy

¹Laboratory of R&D in Engineering Sciences, Faculty of Sciences and Techniques Al-Hoceima, Abdelmalek Essaadi University, Tetouan, Morocco.

^{*} khoudiri.achraf@etu.uae.ac.ma

[†] kelanouz@uae.ac.ma

[‡] eabderrahim@uae.ac.ma

production [28] to study irreversibility over time, and the entropy production rate [29] to analyze the loss of information from the QATM and external system gubits into their reservoirs. We find that the entropy production rate is non-monotonic and attains negative values over time, indicating non-Markovian dynamics, in agreement with Popovic et al. [30], where negative entropy production rate is a signature of non-Markovianity. This motivates us to explore the memory effects of cycles A and B. We quantify non-Markovianity using the measure proposed by Breuer et al. [31] and find that, even with Markovian reservoirs, non-Markovianity arises due to the exchange of correlations between the QATM and the external system over time [15, 30]. To examine the effect of cycles A and B on entanglement generation, we measure the total correlation between the external system qubits using mutual information [32], and concurrence [33] as a measure of entanglement. We find that the total correlation (classical and quantum) is similar in both cycles, but entanglement is generated only when the QATM operates in cycle A. This result reflects the differences between cycles A and B in terms of irreversibility and non-Markovianity over time. Finally, we discuss the effects of correlation coherence [34] and local coherences [35] on entanglement generation, showing that coherence serves as a quantum resource for producing quantum correlations over time in both cycles.

Regarding the experimental framework, our work considers only the theoretical framework, but we set all the parameters in a suitable way and align with trials and experiments in the context of superconducting qubits [36–38].

Our paper is organized as follows: in Sec. II, we discuss our theoretical model, Hamiltonian description of the QATM and external system, QATM cycles, and temperature and energy constraints in Subsec. II A, Subsec. II B. In Sec. III, we discuss the dynamics of quantum thermodynamics; Subsec. III A covers heat dynamics of the subsystems, QATM qubits and external system qubits, while temperatures, entropy production, and entropy production rate are treated in Subsec. III B and Subsec. III C, respectively. The memory effect of quantum thermal machine cycles and entanglement generation are discussed in Sec. IV. Non-Markovianity is in Subsec. IV A, and entanglement generation and the impact of correlation coherence in Subsec. IV B and Subsec. IV C, respectively, followed by the conclusion.

II. THEORETICAL FRAMEWORK, OPERATION CYCLE OF THE THERMAL MACHINE, AND TEMPERATURE AND ENERGY CONSTRAINTS

Our theoretical model consists of an quantum autonomous thermal machine (QATM) denoted by $M=M_1\otimes M_2$, represented by two non-coupled qubits M_1 and M_2 , each of which is coupled at thermal equilibrium to a

Markovian bosonic reservoir, respectively denoted by R_1 and R_2 , at temperatures T_{R_1} and T_{R_2} respectively. The QATM M is coupled to an external system $S = S_1 \otimes S_2$, represented by two non-coupled qubits denoted by S_1 and S_2 , respectively, as shown in Fig. 1.

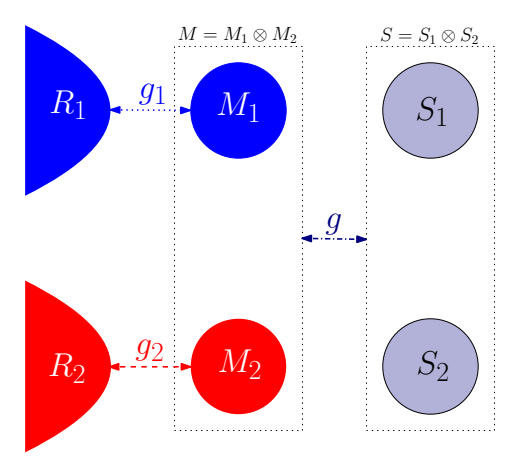


FIG. 1. Diagram of the QATM $M = M_1 \otimes M_2$ coupled to the external system $S = S_1 \otimes S_2$ via a coupling coefficient g. R_1 and R_2 are the bosonic reservoirs of the QATM qubits M_1 and M_2 , respectively.

We will investigate the Hilbert space structure of the QATM M and the external system S, as well as the difference between the temperatures T_{R_1} and T_{R_2} , to realize a thermodynamic cycles on the QATM. In this way, we can investigate how to boost the memory effects in the external system S, and enhance the generation and control of entanglement.

A. Hamiltonian Framework and System Dynamics

The total Hamiltonian of our theoretical model is represented in the following compact form,

$$\hat{H} = \hat{H}_M + \hat{H}_S + \hat{H}_R + \hat{H}_{MR} + \hat{H}_{MS},\tag{1}$$

where \hat{H}_m , for $m = \{M, S, R\}$, is the free Hamiltonian of the QATM M, the external system S, and the reservoirs $R = R_1 \otimes R_2$, respectively. Specifically,

$$\begin{split} \hat{H}_{M} &= \sum_{i=1}^{2} \hat{H}_{M_{i}}, \quad \hat{H}_{M_{i}} = E_{M_{i}} \hat{\sigma}_{M_{i}}^{\dagger} \hat{\sigma}_{M_{i}}, \\ \hat{H}_{S} &= \sum_{i=1}^{2} \hat{H}_{S_{i}}, \quad \hat{H}_{S_{i}} = E_{S_{i}} \hat{\sigma}_{S_{i}}^{\dagger} \hat{\sigma}_{S_{i}}, \\ \hat{H}_{R} &= \sum_{i=1}^{2} \hat{H}_{R_{i}}, \quad \hat{H}_{R_{i}} = \sum_{k} E_{R_{ik}} \hat{a}_{R_{ik}}^{\dagger} \hat{a}_{R_{ik}}. \end{split}$$

where E_{M_i} and E_{S_i} for $i = \{1, 2\}$ are the spacing energy of the QATM qubits $M_1(M_2)$ and the external system subits $S_1(S_2)$ respectively. $E_{R_{ik}}$ is the spacing energy of

the reservoir R_i for $i=\{1,2\}$ for each mode k of the set of bosonics harmonic oscillators. The raising and lowering operators of the QATM and the external system qubits M_i and S_i are defined as $\hat{\sigma}_{M_i(S_i)} = |0\rangle_{M_i(S_i)} \langle 1|$ and $\hat{\sigma}_{M_i(S_i)}^{\dagger} = |1\rangle_{M_i(S_i)} \langle 0|$, and realize the operations $\hat{\sigma}_{M_i(S_i)} |1\rangle_{M_i(S_i)} = |0\rangle_{M_i(S_i)}$ and $\hat{\sigma}_{M_i(S_i)}^{\dagger} |0\rangle_{M_i(S_i)} = |1\rangle_{M_i(S_i)}$, respectively, for $i=\{1,2\}$. $\hat{a}_{R_{ik}}$ ($\hat{a}_{R_{ik}}^{\dagger}$) are the annihilation and creation operators of the reservoir R_i for the harmonic oscillator mode k.

The interaction between each reservoir R_1 (R_2) and the QATM qubits M_1 (M_2) is described, under the rotating wave approximation ($E_{M_i} = E_{R_{ik}}$), by the interaction Hamiltonian \hat{H}_{MR} , defined as:

$$\hat{H}_{MR} = \sum_{i=1}^{2} \sum_{k} g_{ik} (\hat{\sigma}_{M_i} \hat{a}_{ik}^{\dagger} + H.c), \tag{2}$$

Here, g_{ik} is the coupling rate between the reservoir R_i and the qubit M_i for $i = \{1, 2\}$.

The Hamiltonian \hat{H}_{MS} represents the interaction between the QATM $M = M_1 \otimes M_2$ and the external system $S = S_1 \otimes S_2$, and is described by

$$\hat{H}_{MS} = g \left(|0_{M_1} 1_{M_2} 1_{S_1} 0_{S_2} \rangle \langle 1_{M_1} 0_{M_2} 0_{S_1} 1_{S_2} | + H.c. \right), \tag{3}$$

where g denotes the coupling coefficient between the QATM M and the external system S. The interaction Hamiltonian \hat{H}_{MS} induces the transitions $|0_{M_1}1_{M_2}\rangle \otimes |1_{S_1}0_{S_2}\rangle \leftrightarrow |1_{M_1}0_{M_2}\rangle \otimes |0_{S_1}1_{S_2}\rangle$ under the condition of energy conservation[11],

$$E_{M_2} - E_{M_1} = E_{S_2} - E_{S_1}, (4)$$

This resonance condition between M and S drives the transitions in M, $|0_{M_1}1_{M_2}\rangle \leftrightarrow |1_{M_1}0_{M_2}\rangle$, and in S, $|1_{S_1}0_{S_2}\rangle \leftrightarrow |0_{S_1}1_{S_2}\rangle$, through the exchange of an energy quantum $E_M=E_S=E_{M_2}-E_{M_1}$, with $E_{M_2}>E_{M_1}$ and $E_{S_2}>E_{S_1}$. According to this interaction, the quantum thermodynamic cycles of the QATM will be defined in the next subsection.

The initial state of our total theoretical model, denoted by $\hat{\rho}(0)$, is defined as follows:

$$\hat{\rho}(0) = \hat{\rho}_{R1-M1}(0) \otimes \hat{\rho}_{R_2-M_2}(0) \otimes \hat{\rho}_S(0), \tag{5}$$

Initially, we consider no correlation between each subsystem, and $\hat{\rho}_{R_i-M_i}(0) = \hat{\rho}_{R_i}(0) \otimes \hat{\rho}_{M_i}(0)$ for $i = \{1, 2\}$, where $\hat{\rho}_{R_i}(0)$ and $\hat{\rho}_{M_i}(0)$ are the initial states of the subsystems R_i and M_i , respectively. The initial state of the external system is given by $\hat{\rho}_S(0) = \hat{\rho}_{S_1}(0) \otimes \hat{\rho}_{S_2}(0)$.

Under the weak interaction between the QATM $M = M_1 \otimes M_2$ and the reservoirs R_1 and R_2 , the total system evolves as $\hat{\rho}(t) = \hat{U}(t)\hat{\rho}(0)\hat{U}^{\dagger}(t)$, where $\hat{U}(t) = \exp(-i\hat{H}t)$ (with $\hbar = 1$). The reduced state of the subsystems M and S is then obtained as

$$\hat{\rho}_{MS}(t) = \text{Tr}_{R_1, R_2} \{ \hat{\rho}(t) \}.$$
 (6)

. Hence, one can use the local standard Born-Markov master equation in Lindblad form[39, 40]:

$$\frac{d}{dt}\hat{\rho}_{MS}(t) = -j\left[\hat{H}_S + \hat{H}_M, \hat{\rho}_{MS}(t)\right] + \mathcal{L}[\hat{\rho}_{MS}(t)], \quad (7)$$

where $-j \left[\hat{H}_S + \hat{H}_M, \hat{\rho}_{MS}(t) \right]$, describing the free evolution of the subsystems M and the external system S, is the reversible part of the evolution of our theoretical model, and $\mathcal{L}[\hat{\rho}_{MS}(t)]$ is the dissipative (irreversible) part, describing the decoherence effects of the reservoirs R_1 and R_2 in to M and S, defined as:

$$\mathcal{L}[\hat{\rho}_{MS}(t)] = -j \left[\hat{H}_{MS}, \hat{\rho}_{MS}(t) \right] + \sum_{i=1}^{2} \mathcal{D}^{[T_{M_i}]}[\hat{\rho}_{MS}(t)], \tag{8}$$

$$\mathcal{D}^{[T_{M_i}]}[\hat{\rho}_{MS}(t)] = \gamma_i (\bar{n}_i (T_{M_i}, E_{M_i}) + 1) \mathcal{D}^{[\hat{\sigma}_{M_i}]}[\hat{\rho}_{MS}(t)] + \gamma_i \bar{n}_i (T_{M_i}, E_{M_i}) \mathcal{D}^{[\hat{\sigma}^{\dagger}_{M_m}]}[\hat{\rho}_{MS}(t)],$$

$$\mathcal{D}^{[\hat{\sigma}_{M_i}^{\dagger}]}[\hat{\rho}_{MS}(t)] = \hat{\sigma}_{M_i}^{\dagger}\hat{\rho}_{MS}(t)\hat{\sigma}_{M_i} - \frac{1}{2}\{\hat{\sigma}_{M_i}\hat{\sigma}_{M_i}^{\dagger}, \hat{\rho}_{MS}(t)\},$$

$$\mathcal{D}^{[\hat{\sigma}_{M_i}]}[\hat{\rho}_{MS}(t)] = \hat{\sigma}_{M_i}\hat{\rho}_{MS}(t)\hat{\sigma}_{M_i}^{\dagger} - \frac{1}{2}\{\hat{\sigma}_{M_i}^{\dagger}\hat{\sigma}_{M_i},\hat{\rho}_{MS}(t)\},$$

Here, γ_i denotes the corresponding dissipation rate, and $\bar{n}_i(T_{M_i}, E_{M_i})$ represents the average number of harmonic oscillators in the thermal bosonic reservoir R_i at temperature T_{M_i} , corresponding to the energy gap E_{M_i} , defined as (with $\hbar = 1$),

$$\bar{n}(T_{M_i}, E_{M_i}) = \frac{1}{\exp(\frac{E_{M_i}}{T_{M_i}}) - 1}, \quad \text{for } i = \{1, 2\}.$$
 (9)

It is noted that the coupling between M_i and its corresponding reservoir R_i ($i = \{1, 2\}$) in the Hamiltonian of Eq. 2 satisfies the condition $\gamma_i = \sum_k g_{ik} \ll E_{M_i}$. Similarly, the coupling between M and S fulfills the condition $g \ll E_{M_2}$, which ensures the validity of the weak-coupling limit [39, 40].

B. Quantum Thermal Machine Modeling

The objective of this subsection is to define the QATM M, and to investigate the difference in temperature reservoirs R_1 (R_2) and the Hilbert space structure of each subsystem M and S as a resource to operate the QATM M autonomously without any external injection of work. The QATM qubits M_1 and M_2 are in thermal equilibrium with their respective reservoirs R_1 and R_2 at temperatures $T_{R_i} = T_{M_i}$ for $i = \{1, 2\}$. They are defined by the Boltzmann distribution in their thermal states (Boltzmann constant $K_B = 1$) as

$$\hat{\rho}_{M_i}(0) = \frac{1}{Z_{M_i}} e^{-\frac{\hat{H}_{M_i}}{T_{M_i}}}, \quad i = \{1, 2\},$$

$$\hat{\rho}_{M}(0) = \hat{\rho}_{M_1}(0) \otimes \hat{\rho}_{M_2}(0), \tag{10}$$

here, $Z_{M_i} = Tr_{M_i} \{e^{-\frac{H_{M_i}}{T_{M_i}}}\}$ is the partition function of the thermal machine qubit M_i for $i = \{1, 2\}$, and $\hat{\rho}_M(0)$ is the initial state of the QATM M. Note that the reservoirs R_1 and R_2 are the cold and hot reservoirs, respectively, with $T_{M_1} \leq T_{M_2}$. We set the energy spacing of each qubit M_1 and M_2 such that the condition $E_{M_2} > E_{M_1}$ is satisfied.

Since the total system evolves as $\hat{\rho}(t) = \hat{U}(t)\hat{\rho}(0)\hat{U}^{\dagger}(t)$, according to the first principle of quantum thermodynamics[1–3], the total energy, denoted by $E(t) = \text{Tr}\{\hat{\rho}(t)\hat{H}\}$, is conserved over time $(\Delta E(t) = 0)$. For the subsystems M and S, the internal energy is given by $E_{MS}(t) = \text{Tr}\{(\hat{H}_S + \hat{H}_M)\hat{\rho}_{MS}(t)\}$. According to the first law of quantum thermodynamics, the variation of the internal energy is decomposed into heat and work contributions as

$$\Delta E_{MS}(t) = Q_{MS}(t) + W_{MS}(t),$$

$$Q_{MS}(t) = \text{Tr}_{M,S} \{ (\hat{H}_S + \hat{H}_M) \, \Delta \hat{\rho}_{MS}(t) \},$$

$$W_{MS}(t) = \text{Tr}_{M,S} \{ \hat{\rho}_{MS}(t) \, (\Delta \hat{H}_S + \Delta \hat{H}_M) \},$$
(11)

where $Q_{MS}(t)$ and $W_{MS}(t)$ denote the heat and work, respectively [1–3]. Since the Hamiltonians \hat{H}_M and \hat{H}_S are time-independent, the work contribution zero over time, i.e., $W_{MS}(t) = 0$ [1–3]. In our theoretical model, only heat flux is exchanged between the subsystems, such that

$$Q_{MS}(t) = \sum_{i=1}^{2} Q_{M_i}(t) + Q_S(t),$$

$$Q_{M_i}(t) = \text{Tr}\{\hat{H}_{M_i} \, \Delta \hat{\rho}_{M_i}(t)\},$$

$$Q_S(t) = \text{Tr}\{\hat{H}_S \, \Delta \hat{\rho}_S(t)\},$$
(12)

where $Q_{M_i}(t)$ represents the heat exchanged between M_i and its corresponding reservoir R_i (for $i = \{1, 2\}$), and $Q_S(t)$ denotes the heat exchanged between the external system S and the QATM $M = M_1 \otimes M_2$ over time.

We investigate the interaction between the reservoirs $R_1(R_2)$, the QATM $M=M_1\otimes M_2$, and the external system $S=S_1\otimes S_2$, and the difference between the temperature T_{M_1} and T_{M_2} and the Hilbert space structure of each subsystem S and M to realize two thermodynamical cycles on the QATM M, noted respectively as (Cycle A) and (Cycle B), are defined as follows:

• Cycle A, as shown in Fig. 2a:

- $-|0_{M_1}0_{M_2}\rangle \rightarrow |1_{M_1}0_{M_2}\rangle$ and $|0_{M_1}1_{M_2}\rangle \rightarrow |1_{M_1}1_{M_2}\rangle$, corresponding to heating of M_1 $(Q_{M_1}(t) \geq 0)$;
- $-|1_{M_1}0_{M_2}\rangle \rightarrow |0_{M_1}1_{M_2}\rangle$, where the machine M $(Q_M(t) \geq 0)$ absorbs heat from S, resulting in cooling of S $(Q_S(t) \leq 0)$;
- $\begin{array}{lll} -\mid & 0_{M_1} 1_{M_2} \rangle & \rightarrow \mid & 0_{M_1} 0_{M_2} \rangle & \text{and} & \mid & 1_{M_1} 1_{M_2} \rangle & \rightarrow \\ \mid & 1_{M_1} 0_{M_2} \rangle, & \text{corresponding to cooling of } M_2 \\ & (Q_{M_2}(t) \leq 0). \end{array}$

• Cycle B, as shown in Fig. 2b:

- $-|1_{M_1}0_{M_2}\rangle \rightarrow |0_{M_1}0_{M_2}\rangle$ and $|1_{M_1}1_{M_2}\rangle \rightarrow |0_{M_1}1_{M_2}\rangle$, corresponding to cooling of M_1 $(Q_{M_1}(t) \leq 0)$;
- $-|0_{M_1}1_{M_2}\rangle \rightarrow |1_{M_1}0_{M_2}\rangle$, where the machine M $(Q_M(t) \leq 0)$ releases heat into S, resulting in heating of S $(Q_S(t) \geq 0)$;
- $-|0_{M_1}0_{M_2}\rangle \rightarrow |0_{M_1}1_{M_2}\rangle$ and $|1_{M_1}0_{M_2}\rangle \rightarrow |1_{M_1}1_{M_2}\rangle$, corresponding to heating of M_2 $(Q_{M_2}(t) \geq 0)$.

Remark that we used the concept of a cycle as defined in the context of quantum autonomous thermal machines [11–15]. There is a fundamental difference between the cycles of quantum autonomous thermal machines and those of traditional stroke-based thermal machines, where a cycle is defined by the evolution of external parameters such as bath temperatures [1–3]. In our approach, cycles A and B refer to specific sequences of states that the QATM system goes through, which is consistent with the standard usage in the quantum autonomous setting.

Noted that the QATM $M=M_1\otimes M_2$ and the external system $S=S_1\otimes S_2$ are operated as a single body of energy spacing $E_M=E_S=E_{M_2}-E_{M_1}$, with the ground and excited states being $|0\rangle_{M(S)}=|1_{M_1(S_1)}0_{M_2(S_2)}\rangle$ and $|1\rangle_{M(S)}=|0_{M_1(S_1)}1_{M_2(S_2)}\rangle$, respectively. The populations of the excited and ground states, denoted $P_{M(S)}^E(t)$ and $P_{M(S)}^G(t)$, are defined as:

$$P_{M(S)}^{G}(t) = P_{M_{1}(S_{1})}^{E}(t)P_{M_{2}(S_{2})}^{G}(t), \tag{13}$$

$$P_{M(S)}^{E}(t) = P_{M_1(S_1)}^{G}(t)P_{M_2(S_2)}^{E}(t), \tag{14}$$

where $P_{M_i(S_i)}^G(t) = \langle 0_{M_i(S_i)}|\hat{\rho}_{M_i(S_i)}(t)|0_{M_i(S_i)}\rangle$ and $P_{M_i(S_i)}^E(t) = \langle 1_{M_i(S_i)}|\hat{\rho}_{M_i(S_i)}(t)|1_{M_i(S_i)}\rangle$ are the ground and excited state populations of the qubit $M_i(S_i)$ for $i=\{1,2\}$, respectively. In the context of quantum thermodynamics, the QATM M and the external system S are treated as a single body, namely a virtual qubit. Since the QATM qubits M_1 and M_2 follow Boltzmann distributions, we have:

$$P_{M_i}^E(t) = P_{M_i}^G(t)e^{-\frac{E_{M_i}}{T_{M_i}}}, \quad (i = \{1, 2\}),$$

$$P_M^E(t) = P_M^G(t)e^{-\frac{E_M}{T_M}}, \quad (15)$$

Here, E_M is the energy level spacing of the QATM when treated as a single body, at the virtual temperature denoted T_M , and is defined as:

$$T_M = \frac{E_M}{\frac{E_{M_2}}{T_{M_2}} - \frac{E_{M_1}}{T_{M_1}}},\tag{16}$$

The virtual temperature of the QATM, T_M , is not the average of the temperatures T_{M_1} and T_{M_2} . At equilibrium, we have $T_M = T_{M_1} = T_{M_2}$, and it is an important

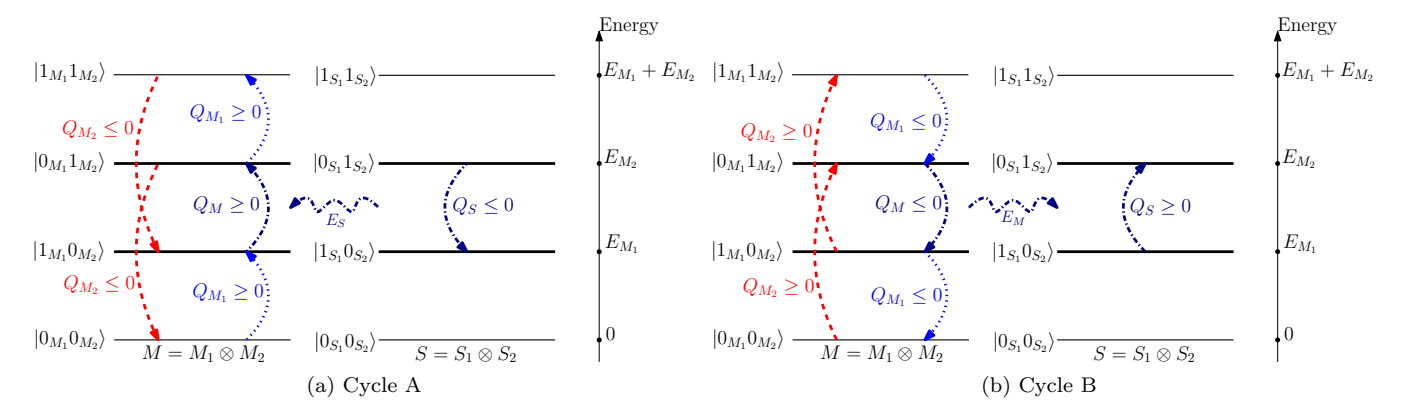


FIG. 2. (a) Schematic representation of QATM cycle A: heating of qubit M_1 and cooling of qubit M_2 with heat transfer from the external system to the machine. (b) Cycle B: heating of qubit M_2 and cooling of qubit M_1 with heat transfer from the machine to the external system. Arrows indicate the direction of heat flow between the qubits, thermal reservoirs, and the external system.

parameter used to define the constraint on temperature that differentiates between cycle A and cycle B.

For the cycles A and B, the cycles are closed under the exchange of heat between the QATM M and the excternal S, corrisponding to the transition $|0\rangle_M \leftrightarrow |1\rangle_M$, with the exchanged heat of the QATM M where act as single body is noted $Q_M(t)$ is defiend as ;

$$Q_M(t) = E_M(P_M^E(t) - P_M^E(0)). (17)$$

• Cycle A consists of heat gain from the external system S into the QATM M, meaning that $Q_M(t) \geq 0$, which implies an increase in the excited state probability of the QATM M ($P_M^E(t) \geq P_M^E(0)$). Using Eq. 15 and Eq. 16, we find that the virtual temperature of the QATM M in cycle A evolves negatively over time, $T_M \leq 0$, and we obtain the constraint on the temperatures T_{M_1} and T_{M_2} for realizing cycle A as:

$$T_{M_1} \le \frac{E_{M_1}}{E_{M_2}} T_{M_2}. \tag{18}$$

• Cycle B consists of heat gain by the external system S from the QATM M, meaning that $Q_M(t) \leq 0$, which implies a decrease in the excited state probability of the QATM M ($P_M^E(t) \leq P_M^E(0)$). Using Eq. 15 and Eq. 16, we find that the virtual temperature of the QATM M in cycle B evolves positively over time, $T_M \geq 0$, and we obtain the constraint on the temperatures T_{M_1} and T_{M_2} for realizing cycle B as:

$$T_{M_1} \ge \frac{E_{M_1}}{E_{M_2}} T_{M_2}. \tag{19}$$

Theoretically, we show that the constraints on the energies of the QATM qubits and the external system qubits satisfy the conditions in Eq. 4. In the remainder of the paper, for simplicity, we set $E_{M_i} = E_{S_i}$ for $i = \{1,2\}$. The temperature constraints required to realize the transition between cycles A and B are given by Eq. 18 and Eq. 19. It should be noted that the autonomy of the QATM refers to the fact that the machine operates without any external time-dependent control. Once initialized, the QATM qubits M_1 and M_2 interact with their respective reservoirs and with the external system qubits S_1 and S_2 through fixed Hamiltonian interactions. All energy exchanges and the generation of virtual temperatures occur purely due to these time-independent interactions, so the machine functions continuously and autonomously, without requiring external driving or modulation.

For the numerical results, we normalize the energy scale by setting $E_{M_2} = 10$ and choose $E_{M_1} = 0.5 E_{M_2} = 5$, with dissipation rates $\gamma_i = 0.01 E_{M_i}$ for $i = \{1, 2\}$. The transition point between Cycles A and B, in terms of temperature, occurs at

$$T_{M_1} = \frac{E_{M_1}}{E_{M_2}} T_{M_2} = 0.5 T_{M_2}.$$

In the simulations, we use $T_{M_1}=0.1T_{M_2}$ for Cycle A and $T_{M_1}=0.8T_{M_2}$ for Cycle B, with $T_{M_2}=E_{M_2}=10$, The range of the coupling between the QATM M and the external system $S,\ g=0.03E_{M_2},\ 0.05E_{M_2},\ 0.07E_{M_2},$ and $0.09E_{M_2}.$

Moreover, these parameters are used to map between the theoretical framework and the experimental realization. For instance, in superconducting qubits [36–38], the energy spacing typically lies between 4 GHz and 10 GHz. In natural units ($\hbar=1$), using $E_{M_2}=10$ is equivalent to operating in the GHz range, and the coupling g in experimental studies ranges between 10 MHz and 100 MHz,and the relevant time scale lies between 20 μ s and 200 μ s. Which proves that our model is experimentally realizable and represents a realistic system.

III. DYNAMICS OF QUANTUM THERMODYNAMIC QUANTITIES: HEAT AND TEMPERATURE

In this section, we numerically manipulate the constraints provided in Eq. 18 and Eq. 19 on the dynamics of heat of each subsystem and on the dynamics of temperatures. We used, as the initial state for the QATM M, the density matrix in Eq. 10. For the external system S, in the remainder of the paper, we use the superposition state $|\psi(0)\rangle_{S_1} = \frac{1}{\sqrt{2}}(|0\rangle_{S_1} + |1\rangle_{S_1})$ for qubit S_1 , and the superposition state $|\psi(0)\rangle_{S_2} = \frac{1}{\sqrt{2}}(|0\rangle_{S_2} - |1\rangle_{S_2})$ for qubit S_2 . The corresponding initial density matrix is given by $\hat{\rho}_{S_i}(0) = |\psi(0)\rangle_{S_i} \langle \psi(0)|$ for $i = \{1, 2\}$.

A. Heat dynamics

We investigate the definition of heat in Eq. ??, to show the dynamics of heat for the QATM qubits M_1 and M_2 , $Q_{M_1}(t)$ and $Q_{M_2}(t)$ respectively, and for the external system qubits S_1 and S_2 , $Q_{S_1}(t)$ and $Q_{S_2}(t)$ respectively. We set the coupling between the QATM M and the external system S to g = 0.09, and the temperature of the qubit M_2 to $T_{M_2} = 1$, and we vary the heats as a function of time and the temperature T_{M_1} in the interval $T_{M_1} \in [0.1T_{M_2}, T_{M_2}]$ as a contour plot.

The variations of heat for the QATM qubits, $Q_{M_1}(t)$ and $Q_{M_2}(t)$, are shown in Fig. 3a and Fig. 3b, respectively. We observe that in the case where $T_{M_1} \leq 0.5T_{M_2}$, the heat satisfies $Q_{M_1}(t) \geq 0$ and $Q_{M_2}(t) \leq 0$, and in the case $T_{M_1} \geq 0.5T_{M_2}$, the heat satisfies $Q_{M_1}(t) \leq 0$ and $Q_{M_2}(t) \geq 0$. Physically, this behavior corresponds to the conditions of transition between cycles A and B in Eq. 18 and Eq. 19.

For the external system qubits S_1 and S_2 , the heat variations are given in Fig. 3c and Fig. 3d, respectively. In the case $T_{M_1} \leq 0.5T_{M_2}$ (cycle A), the heats satisfy $Q_{S_1}(t) \leq 0$ and $Q_{S_2}(t) \geq 0$, and in the case $T_{M_1} \geq 0.5T_{M_2}$ (cycle B), the heats satisfy $Q_{S_1}(t) \geq 0$ and $Q_{S_2}(t) \leq 0$. In connection with the variation of the QATM qubits' heat $Q_{M_i}(t)$ for $i \in \{1,2\}$, under the condition of resonance between the qubits M_i and S_i ($E_{M_i} = E_{S_i}$), the heat is partially exchanged as $Q_{S_i}(t) \rightarrow Q_{M_i}(t)$ for cycle A, and $Q_{M_i}(t) \rightarrow Q_{S_i}(t)$ for cycle B.

The non-monotonic behavior of the heat dynamics for $Q_{M_i}(t)$ and $Q_{S_i}(t)$ is due to the memory effect in our theoretical model, as we will show in the next section (QATM cycles effect on the non-Markovianity).

B. Temperature dynamics

To show the dynamics of the temperatures of the QATM qubits T_{M_i} for the qubits M_i with $i \in \{1, 2\}$, and the virtual temperature of the QATM T_M , we investigate

Eq. 15. We obtain

$$T_{M_i}(t) = \frac{E_{M_i}}{\ln(P_{M_i}^G(t)) - \ln(P_{M_i}^E(t))}, \quad (i \in \{1, 2\}),$$

$$T_M(t) = \frac{E_M}{\ln(P_M^G(t)) - \ln(P_M^E(t))}.$$
(20)

For cycle A in Fig. 4a, initially $T_{M_1}=0.1T_{M_2}$ and $T_{M_2}=1$, and $T_M\leq 0$. Over time, the temperature of qubit M_1 increases, while that of M_2 decreases, in connection with the heat transfer shown in Fig. 3a and Fig. 3b, under the condition given in Eq. 18. Physically, during the transition of qubit M_1 from $|0\rangle_{M_1}$ to $|1\rangle_{M_1}$, it gains positive heat $Q_{M_1}(t)\neq 0$ from its reservoir R_1 , whereas qubit M_2 , during the transition from $|1\rangle_{M_2}$ to $|0\rangle_{M_2}$, loses heat $Q_{M_2}(t)\leq 0$ to its reservoir R_2 . The QATM M gains heat $Q_M\geq 0$ from the external system S at the virtual temperature T_v .

For cycle B in Fig. 4b, initially $T_{M_1} = 0.8T_{M_2}$ and $T_{M_2} = 1$, and $T_M \geq 0$. Over time, the temperature of qubit M_1 decreases under the exchange of positive heat $Q_{M_1}(t) \geq 0$ with its reservoir R_1 (cooling), and the temperature of qubit M_2 increases under the exchange of negative heat $Q_{M_2}(t) \leq 0$ with its reservoir R_2 (heating), satisfying the condition in Eq. 19.

The non-monotonic evolution of the qubit temperatures under increasing coupling between the QATM M and the external system S is due to the memory effect, which consists of information exchange between the QATM and the external system. Note that the virtual temperature can be negative; this is not unphysical, as it is associated with population inversion (as in lasers). The virtual temperature plays a very important role in complex quantum thermodynamic systems, allowing for differentiation between types of thermal machines.

C. Production entropy and production entropy

The quantum production entropy and the production entropy rate, denoted respectively by $\Sigma(t)$ and $\dot{\Sigma}(t)$, are general concepts in quantum thermodynamics. They quantify the irreversibility of the open system over time and can also be interpreted as the loss of information of the system to its environment. Mathematically are defined as

$$\Sigma(t) = \Delta S(\hat{\rho}(t)) - \sum_{i=1}^{2} \frac{\Delta Q_{M_i}(t)}{T_{M_i}(t)}, \qquad (21)$$

$$\sigma(t) = \frac{d}{dt}\Sigma(t),\tag{22}$$

Here, $S(\hat{\rho}(t)) = -\text{Tr}\{\hat{\rho}(t)\log_2[\hat{\rho}(t)]\}$ denotes the von Neumann entropy of the total density matrix of our theoretical model. We define $\Delta S(\hat{\rho}(t)) = S(\hat{\rho}(t)) - S(\hat{\rho}(0))$

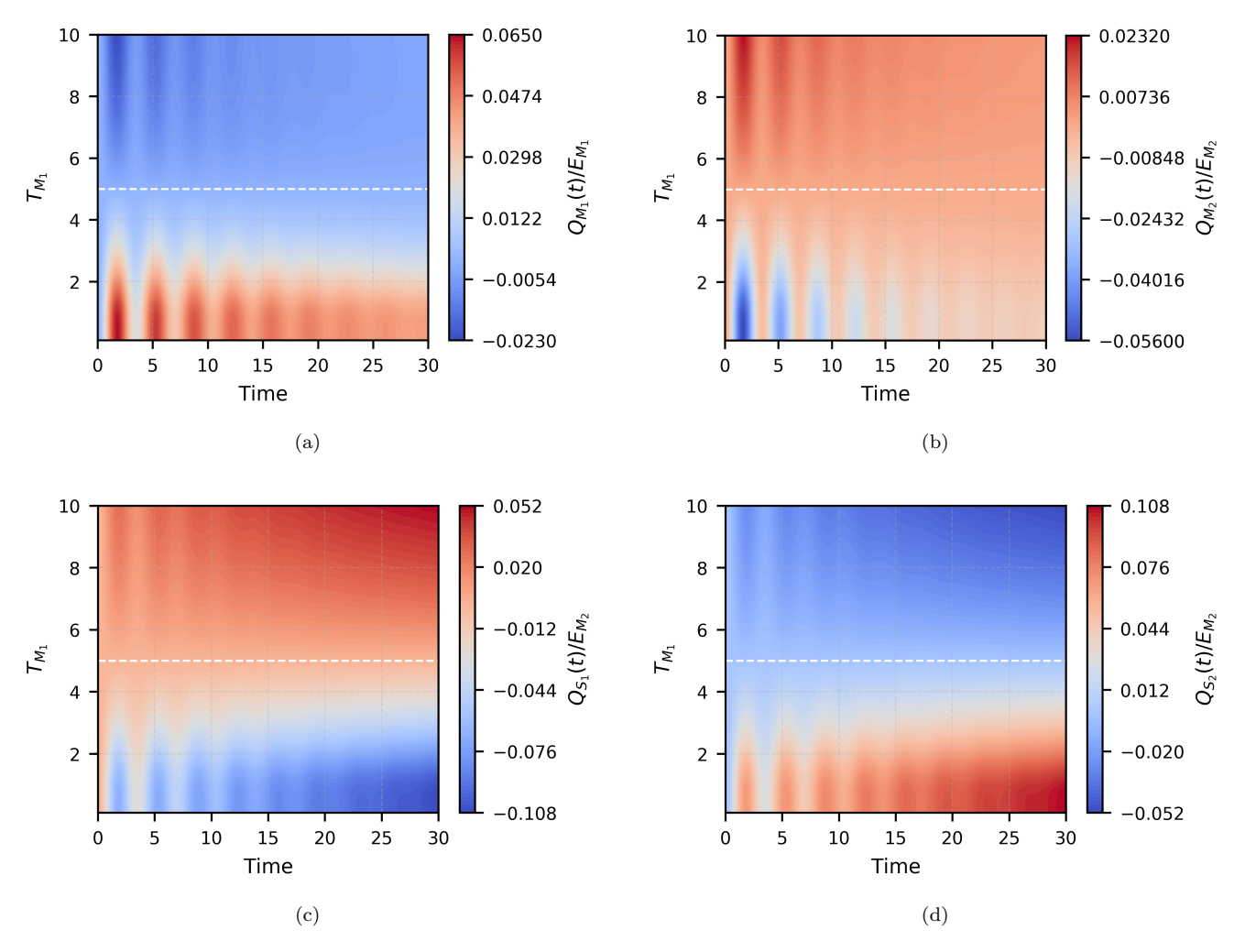


FIG. 3. Heat dynamics for each qubit in the QATM and in the external system. (a,b) Heat exchanged $Q_{M_1}(t)$ and $Q_{M_2}(t)$ for the QATM qubits. (c,d) Heat exchanged $Q_{S_1}(t)$ and $Q_{S_2}(t)$ for the external system qubits. The two regions separated by the white dashed line correspond to the conditions of cycles A and B according to the ratio T_{M_1}/T_{M_2} , we set $T_{M_2} = E_{M_2}$, and $g = 0.08E_{M_2}$.

and $\Delta Q_{M_i}(t) = Q_{M_i}(t) - Q_{M_i}(0) = Q_{M_i}(t)$ for the thermal machine qubit M_i , with $i = \{1, 2\}$.

In Fig. 5, we analyze the entropy production and entropy production rate as functions of time and the coupling strength between the QATM M and the external system S, for cycles A and B shown in Fig. 5a and Fig. 5b, respectively. For both cycles A and B, the entropy production $\Sigma(t)$ remains positive over time. Moreover, the entropy production in cycle A is smaller than that in cycle B over time. Physically, this indicates that the irreversibility of the total systems increases over time and that the decoherence effects of the reservoirs R_1 and R_2 are more pronounced in cycle B than in cycle A; that means the loss of information of the systems QATM and the external system is more remarkable in cycle B than in cycle A.

For the entropy production rate $\sigma(t)$, we observe a nonmonotonic evolution over time for both cycles A and B. In addition, $\sigma(t)$ takes negative values during the evolution. Moreover, in cycle A, $\sigma(t)$ assumes negative values more frequently and with greater magnitude than in cycle B. Physically, negative values of the entropy production rate, i.e., $\sigma(t) < 0$, indicate the presence of non-Markovian dynamics during the evolution of the total system $M \otimes S$. Therefore, as previously mentioned, the fact that $\sigma(t)$ attains more negative values in cycle A suggests that the dynamics are more non-Markovian in cycle A than in cycle B. Furthermore, increasing the coupling strength g between the QATM M and the external system S enhances the non-Markovian behavior, as larger g leads to more pronounced negative values of $\sigma(t)$ compared to smaller g.

In the next section, we will examine the effect of the QATM cycle on the dynamics of the external system $S = S_1 \otimes S_2$, identify the source of non-Markovianity, and discuss the impact of these results on entanglement

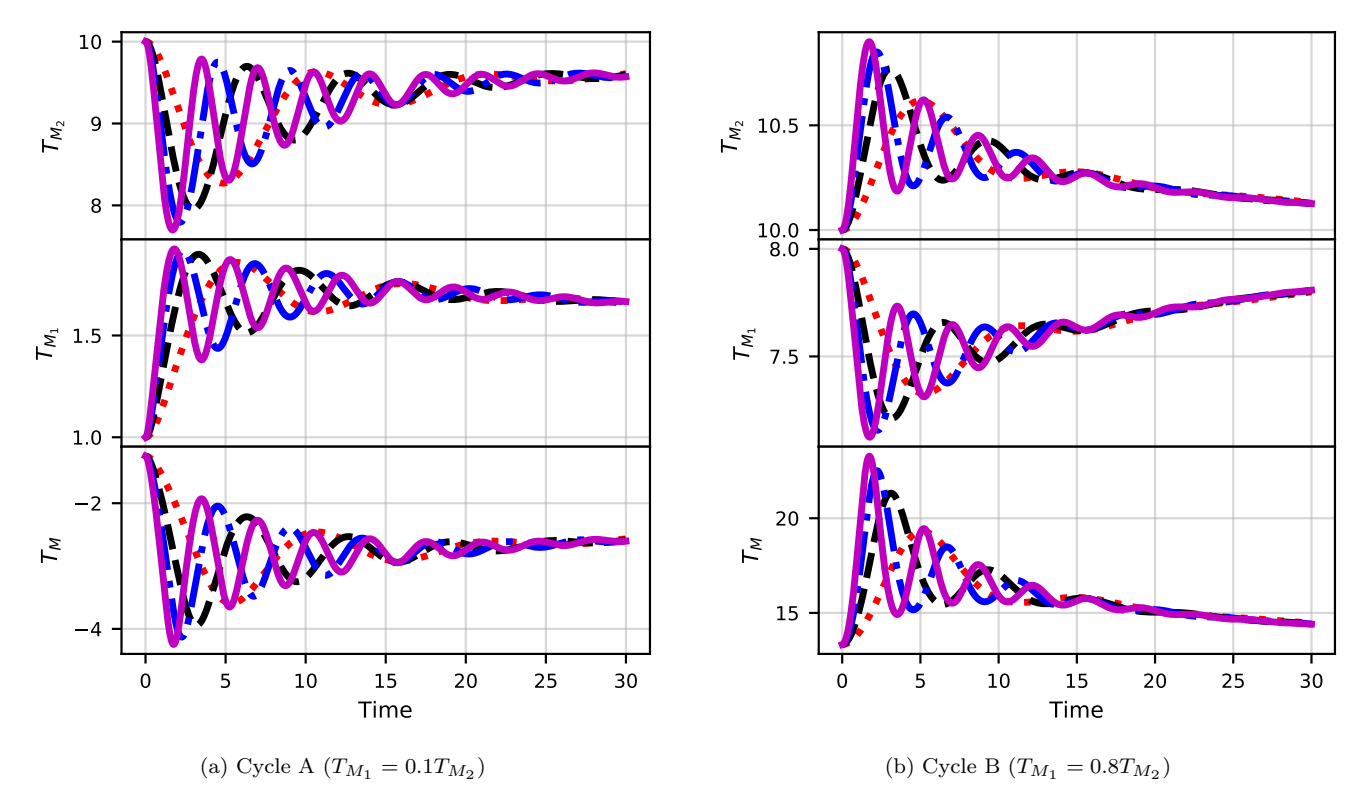


FIG. 4. Temperature evolution of the QATM qubits over time. (a) Cycle A: gradual increase of T_{M_1} and decrease of T_{M_2} with a negative virtual temperature $T_M < 0$. (b) Cycle B: decrease of T_{M_1} and increase of T_{M_2} with a positive virtual temperature $T_M > 0$. The coupling strength is varied as g = 0.03, 0.05, 0.07, and 0.09 (in units of E_{M_2}), represented by red (dotted), black (dashed), blue (dot-dashed), and magenta (solid) curves.

generation in the external system S.

IV. IMPACT OF MEMORY EFFECTS ON ENTANGLEMENT GENERATION IN QATM CYCLES FOR EXTERNAL SYSTEM QUBITS

As discussed previously, indications of non-Markovianity are observed through the oscillations in heat transfer, the temperature evolution of the QATM qubit, and the negative values of the entropy production rate. In this section, we investigate the source of non-Markovianity and analyze the effect of QATM cycles A and B on entanglement generation and the role of coherence in the external system S.

A. Non-Markovianity and correlation exchanges between the QATM and the external system

In our paper [15], we show that the QATM is capable of inducing a backflow of information (non-Markovianity) in the external system through the exchange of correlations between them. Similarly, the work by Popovic *et al.* [30] demonstrates that non-Markovianity can emerge from the exchange of correlations between subsystems.In our

scenario, we quantify non-Markovianity using the measure proposed by Breuer et al. [31], denoted by $\mathcal{N}_m(t)$, which is based on the distinguishability between two quantum states $\hat{\rho}_m^{\alpha}(t)$ and $\hat{\rho}_m^{\beta}(t)$, for $m = \{M, S_1, S_2\}$. Mathematically, it is defined as

$$\mathcal{N}_m(t) = \max_{\hat{\rho}_m^{\alpha\beta}(0)} \int_{\vartheta_m(t)>0} dt \,\vartheta_m(t), \tag{23}$$

where $\hat{\rho}_m^{\alpha\beta}(0) = \hat{\rho}_m^{\alpha}(0) - \hat{\rho}_m^{\beta}(0)$, and $\vartheta_m(t) = \frac{d}{dt} \|\hat{\rho}_m^{\alpha\beta}(t)\|$ is the time derivative of the trace distance between $\hat{\rho}_m^{\alpha}(t)$ and $\hat{\rho}_m^{\beta}(t)$. We quantify the correlation between the QATM $M = M_1 \otimes M_2$ and the external system $S = S_1 \otimes S_2$ using the quantum mutual information [32], denoted by $\mathcal{I}_{M \otimes S}(t)$, which is mathematically defined as

$$\mathcal{I}_{M\otimes S}(t) = S(\hat{\rho}_M(t)) + S(\hat{\rho}_S(t)) - S(\hat{\rho}(t)), \qquad (24)$$

where $S(\hat{\rho}_m(t))$ is the Von Neumann entropy of subsystem $m = \{M, S\}$. For the initial state of the QATM M, we set $\hat{\rho}_M^{\alpha}(0) = \hat{\rho}_M^{\beta}(0) = \hat{\rho}_M(0)$, which is the same state used in Eq. 10. For the external system S, we take $\hat{\rho}_S^{\alpha}(0) = \hat{\rho}_S(0)$ and $\hat{\rho}_S^{\beta}(0) = \bar{\rho}_S(0)$, where $\hat{\rho}_S(0)$ is the

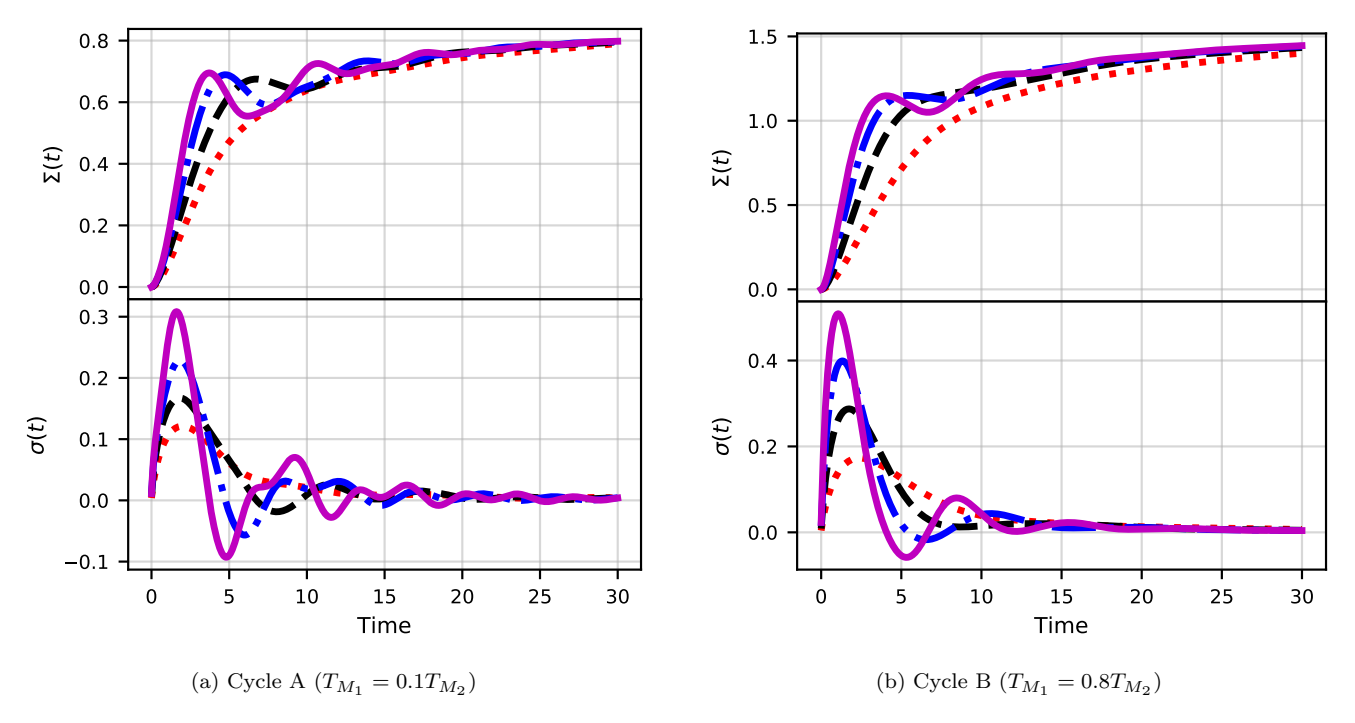


FIG. 5. Entropy production $\Sigma(t)$ and entropy production rate $\sigma(t)$ over time. (a) Cycle A: smaller entropy production with more frequent and stronger negative rates, indicating stronger non-Markovianity. (b) Cycle B: larger entropy production with less frequent negative rates, indicating weaker non-Markovianity. The coupling strength is varied as g = 0.03, 0.05, 0.07, and 0.09 (in units of E_{M_2}), represented by red (dotted), black (dashed), blue (dot-dashed), and magenta (solid) curves.

same state used in Sec. III. The state $\bar{\rho}_S(0)$ is given by

$$\bar{\rho}_S(0) = \sum_{n_{S_1}, n_{S_2} = 0}^{1} \left\langle n_{S_1} n_{S_2} | \hat{\rho}_S(0) | n_{S_1} n_{S_2} \right\rangle \left| n_{S_1} n_{S_2} \right\rangle \left\langle n_{S_1} n_{S_2} \right|,$$
(25)

which represents the fully dephased (incoherent) state of the external system S in the computational basis.

In Fig. 6, we analyze the non-Markovianity measures $\mathcal{N}_M(t)$, $\mathcal{N}_{S_1}(t)$, and $\mathcal{N}_S(t)$ for the QATM M and the external system qubits S_1 and S_2 , respectively, along with the mutual information $\mathcal{I}_{M\otimes S}(t)$ between M and S as functions of time and the coupling strength g. These results are presented for both cycles A and B in Fig. 6a and Fig. 6b, respectively. For both cycles A and B, we observe that where the coupling increases, we show that the non-Markovianity increases on the subsystems M, S_1 and S_2 , also for the correlation increases under the increasing of the coupling g. Moreover, the non-Markovianity and correlation are higher in the case of cycle A than in cycle B, which proves that negative entropy production rate values are an index of the memory effect on our theoretical model. Also the correlations in cycle A are higher than in cycle B, meaning that cycle A conserves the information of the subsystems more effectively than cycle

As we see, the memory effect in our theoretical model is due to the exchanging of the correlations between the QATM M and the external system S over time, and the

correlation partially preserves the information between the subsystems over time. Here we can say that the QATM reacts as a quantum-structured non-Markovian reservoir with the reservoirs R_1 and R_2 , which means physically that the QATM M acts as a filter of the decoherence effect of the reservoirs into the external system S.

B. Entangelment generaation

To show the effect of the QATM M cycles A and B, on the entanglement generation in the external system S over time. We quantified the entanglement using the concurrence [33], noted $\mathcal{C}_{S_1 \otimes S_2}(t)$, and we quantified the correlation between the external system qubit S_1 and S_2 , using the mutual information [32] noted $\mathcal{I}_{S_1 \otimes S_2}(t)$, mathematically are defiend as

$$C_{S_1 \otimes S_2}(t) = \max[0, \sqrt{\lambda_1}(t) - \sum_{i=1}^4 \lambda_i(t)],$$
 (26)

$$\mathcal{I}_{S_1 \otimes S_2}(t) = S(\hat{\rho}_{S_1}(t)) + S(\hat{\rho}_{S_2}(t)) - S(\hat{\rho}_{S}(t)), \quad (27)$$

where, $\lambda_1(t) \geq \lambda_2(t) \geq \lambda_3(t) \geq \lambda_4(t)$ are eigenvalues of the spin-flipped density matrix $\hat{\rho}_S(t)(\sigma_{S_1}^y \otimes \sigma_{S_2}^y)\hat{\rho}_S^*(t)(\sigma_{S_1}^y \otimes \sigma_{S_2}^y)$, and $S(\hat{\rho}_{S-i}(t))$ is the Von Neumann entropy of the qubit S_i for $i = \{1, 2\}$.

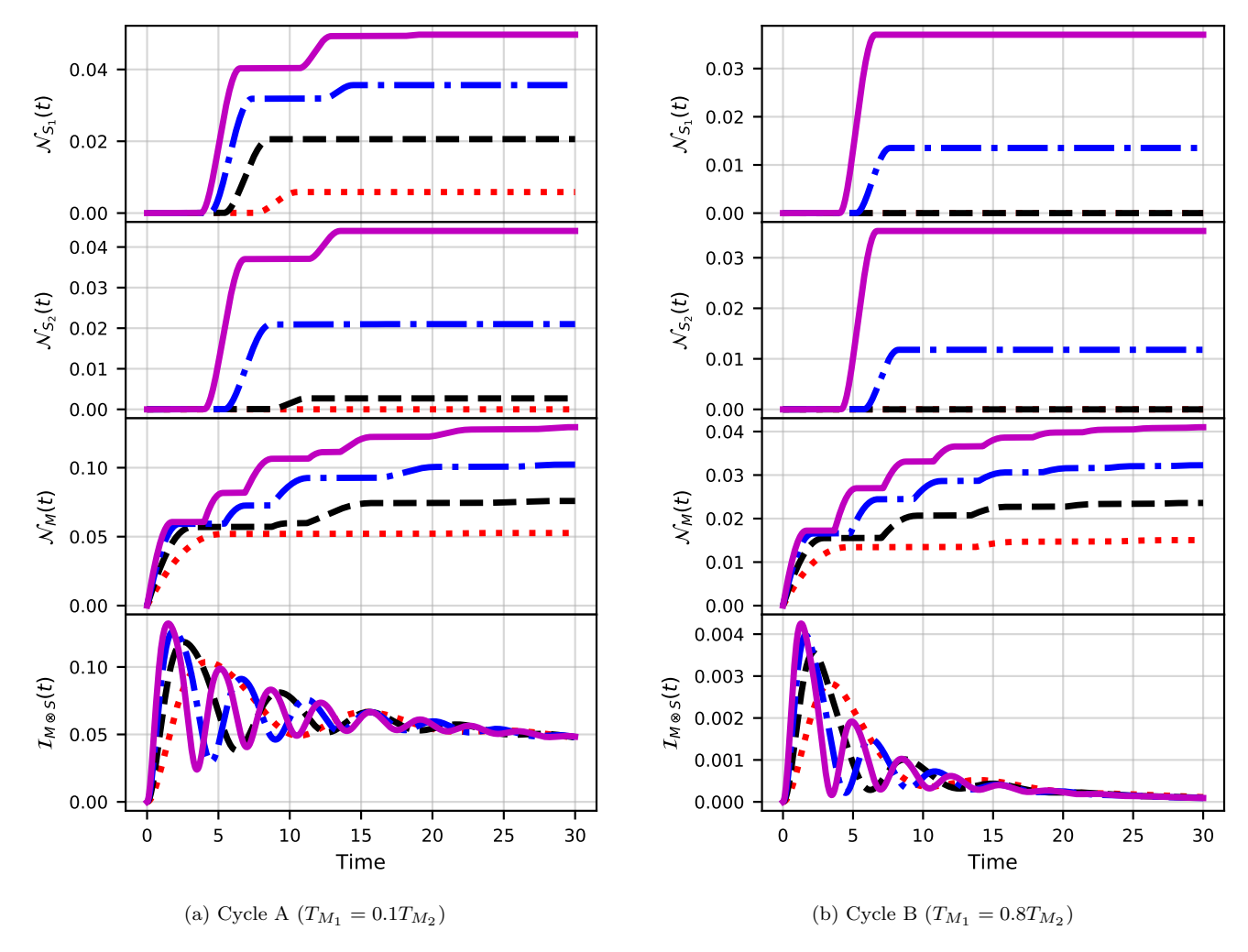


FIG. 6. Non-Markovianity measures and mutual information between the QATM and the external system. (a) Cycle A: higher non-Markovianity in all subsystems and stronger mutual information $I_{M\otimes S}(t)$ as the coupling g increases. (b) Cycle B: lower non-Markovianity and mutual information under the same coupling conditions. The coupling strength is varied as $g=0.03,\,0.05,\,0.07,\,$ and 0.09 (in units of E_{M_2}), represented by red (dotted), black (dashed), blue (dot-dashed), and magenta (solid) curves.

In Fig. 7, we analyzed the entanglement and the correlations in the external system $S=S_1\otimes S_2$ over time. We set the coupling g=0.9, and we manipulate $C_{S_1\otimes S_2}(t)$ and $I_{S_1\otimes S_2}(t)$ versus time and temperature $I_{M_2}\in[0.1T_{M_2},T_{M_2}]$, to show the effect of the QATM I_{M_2} cycles A and B on the entanglement and coherence generation in Fig. 7a and Fig. 7b, respectively.

We observe that if the temperature is below the white dashed line $(T_{M_1} < 0.5T_{M_2}$, cycle A), the concurrence increases as the temperature of qubit M_1 approaches $T_{M_1} = 0.1T_{M_2}$. If the temperature is above the white dashed line $(T_{M_1} \geq 0.5T_{M_2}$, cycle B), the concurrence decreases and approaches zero (very small values) compared to cycle A. In contrast, for the mutual information, we observe that it is symmetric with respect to the white dashed line $(T_{M_1} = 0.5T_{M_2}$, the transition point between cycles A and B). Physically, this means that under the

QATM M operating in cycle A, entanglement is generated, while the total correlation remains the same in both cycles A and B.

In Fig. 7c and Fig. 7d, we manipulate the effect of the coupling g on the dynamics of entanglement and correlation in the external system S, for cycles A and B, respectively. As we said before, the total correlation in both cycles A and B is similar for all values of the coupling g. For the entanglement, we observe that in cycle A, entanglement is generated over time, while in cycle B the concurrence has small values compared to cycle A. For any coupling value g, the concurrence dynamics are close to the same values, but differ only in their monotonic evolution, since g is responsible for the non-Markovian dynamics in our theoretical model.

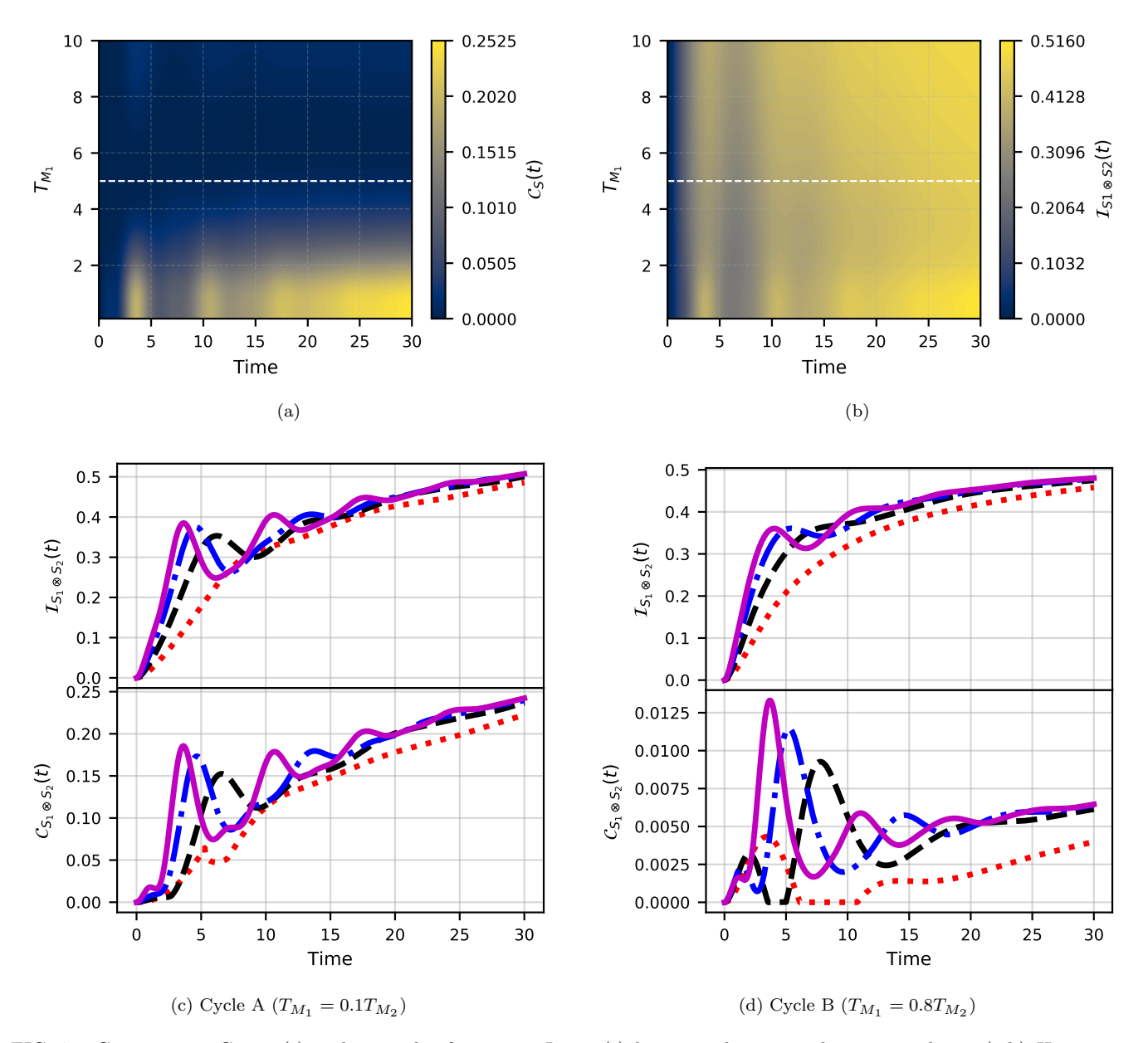


FIG. 7. Concurrence $C_{S_1 \otimes S_2}(t)$ and mutual information $I_{S_1 \otimes S_2}(t)$ between the external system qubits. (a,b) Heat maps as a function of T_{M_1} and T_{M_2} , with the white dashed line separating cycles A and B. (c) Cycle A: noticeable entanglement generation for different coupling values. (d) Cycle B: very weak or vanishing entanglement despite similar total correlations. The coupling strength is varied as g = 0.03, 0.05, 0.07, and 0.09 (in units of E_{M_2}), represented by red (dotted), black (dashed), blue (dot-dashed), and magenta (solid) curves.

C. Role of coherence correlation on entanglement generation

In this part, we shown the role of coherence correlation noted $\Delta C_S(t)$, and the local coherences of the external system qubit on the entanglement generation, for the two cycles A and B of the QATM M. We use the relative entropy of coherence, denoted $C_{S_i}(t)$ for $i = \{1, 2\}$, for the qubits S_1 and S_2 , respectively, and $C_S(t)$ as the global relative entropy of coherence of $S = S_1 \otimes S_2$, which are

mathematically defined as:

$$C_S(t) = S(\bar{\rho}_S(t)) - S(\hat{\rho}_S(t)), \tag{28}$$

$$C_{S_i}(t) = S(\bar{\rho}_{S_i}(t)) - S(\hat{\rho}_{S_i}(t)), \quad i = \{1, 2\},$$
 (29)

$$\Delta C_S(t) = C_S(t) - \sum_{i=1}^{2} C_{S_i}(t), \tag{30}$$

where $S(\bar{\rho}_S(t))$ and $S(\bar{\rho}_{S_i}(t))$ are the von Neumann entropies of the fully dephased states of the global system

S and the local systems S_i for $i = \{1, 2\}$.

In Fig. 8, we analyze the role of coherence correlation $\Delta C_S(t)$ and local coherences $C_{S_i}(t)$ for $i=\{1,2\}$ as functions of time and the coupling between the QATM and the external system, for cycles A and B, shown in Fig. 8a and Fig. 8b, respectively. We observe that for both cycles A and B, the local coherences of the qubits S_1 and S_2 decrease non-monotonically, which physically means that there are memory effects during the coherence evolution. Moreover, the local coherence of the external subsystem in cycle B decays to zero more quickly than in cycle A, due to the higher presence of non-Markovianity in the case of cycle A.

For the coherence correlation $\Delta C_S(t)$, we observe that it increases non-monotonically over time for both cycles, which means that the global coherence of the total external system S is larger than the local coherences of the external subsystems S_1 and S_2 , respectively, i.e., $C_S(t) > \sum_{i=1}^2 C_{S_i}(t)$. This is due to the exchange of coherence correlation between the qubits S_1 and S_2 over time. Physically, there is a relation between the total correlations (classical and quantum), quantified by the mutual information $\mathcal{I}_{S_1 \otimes S_2}(t)$, and the coherence correlation $\Delta C_S(t)$, which is given mathematically by:

$$\Delta C_S(t) = \mathcal{I}_{S_1 \otimes S_2}(t) - \bar{\mathcal{I}}_{S_1 \otimes S_2}(t), \tag{31}$$

Here, $\bar{\mathcal{I}}_{S_1\otimes S_2}(t)=\sum_{i=1}^2 S(\bar{\rho}_{S_i}(t))-S(\bar{\rho}_S(t))$ denotes the classical mutual information between the subsystems S_1 and S_2 , computed from the fully dephased states. This clearly show the role of coherence correlation in the creation of quantum correlations between S_1 and S_2 over time. Moreover, if the external systems S_1 and S_2 , are incoherent, we have mathematically, $\mathcal{I}_{S_1\otimes S_2}(t)=\bar{\mathcal{I}}_{S_1\otimes S_2}(t)$, means that the coherence correlation $\Delta C_S(t)=0$, and consequently, the concurrence is also zero. This highlights the fact that entanglement is directly linked to coherence correlations. This confirms that the external system qubits were initially prepared in superposition states.

V. DISCUSSION AND CONCLUSION

This work explores, in a general context, the relationship between quantum thermodynamics theory in the framework of quantum thermal machines and quantum information theory in the frameworks of entanglement and non-Markovianity. We studied the effect of the quantum autonomous thermal machine on entanglement generation, considering the Hilbert space structure, temperatures, correlation exchange, memory effects, and correlation coherence as a quantum resource. We show how the virtual temperature and energy spacing of the QATM and the external system qubits are investigated to realize thermodynamical cycles A and B, demonstrating their effects on non-Markovianity and entanglement generation.

We study a quantum autonomous thermal machine (QATM) composed of two qubits, M_1 and M_2 , each cou-

pled in thermal equilibrium with its own bosonic Markovian reservoir, R_1 and R_2 , at different temperatures. The external system, denoted by S, consists of two noncoupled qubits, S_1 and S_2 . We investigate the Hilbert space structure and the notion of virtual temperature to realize a common coupling between QATM M and external system S. We provide the temperature and energy constraints necessary to realize thermodynamical cycles of QATM M. Two cycles, A and B, are represented, with the transition temperature between cycles given by $T_{M_1} = \frac{E_{M_2}}{E_{M_1}} T_{M_2}$.

We numerically demonstrate the robustness of our theoretical model by analyzing the QATM cycles based on heat exchange between QATM qubits M_1 , M_2 and external system qubits S_1 , S_2 , and on the temperatures T_{M_1} and T_{M_2} over time. The transition from cycle A to B is characterized by the transition temperature $T_{M_1} = \frac{E_{M_2}}{E_{M_1}} T_{M_2}$. We analyze the second law of quantum thermodynamics via entropy production, showing that irreversibility in cycle A is smaller than in cycle B, indicating that cycle A suppresses reservoir decoherence more efficiently.

The entropy production rate can take negative values during evolution, indicating memory effects. We assess non-Markovianity, showing it is more pronounced in cycle A than cycle B, especially in external qubits S_1 and S_2 . This non-Markovianity results from correlation exchange where QATM acts as a structured non-Markovian reservoir for S.

Entanglement is generated in S only when QATM operates in cycle A, due to lower irreversibility and higher non-Markovianity compared to cycle B. Total correlation remains the same in both cycles as it relates to global properties of S. Cycle A controls reservoir decoherence on S more effectively than cycle B. Correlation coherence is an essential resource for entanglement generation in S, since incoherent S states imply vanishing correlation coherence.

In relation to literature, Khandelwal et al. [7] and Brask et al. [8] investigate QATM for entanglement steady-state generation considering only steady-state QATM effects without external system or memory effects. Aguilar et al. [10] consider thermal machine entanglement in different environments but neglect memory effects of autonomous thermal machines. Our model considers QATM in non-equilibrium and its effect on external system with memory effects and Hilbert space structure to realize thermodynamical cycles, generalizing [15] by exploring entanglement generation and quantum thermodynamic cycles beyond steady state.

Our theoretical model is suitable for superconducting qubit platforms, as parameters align with those used in existing experimental works.

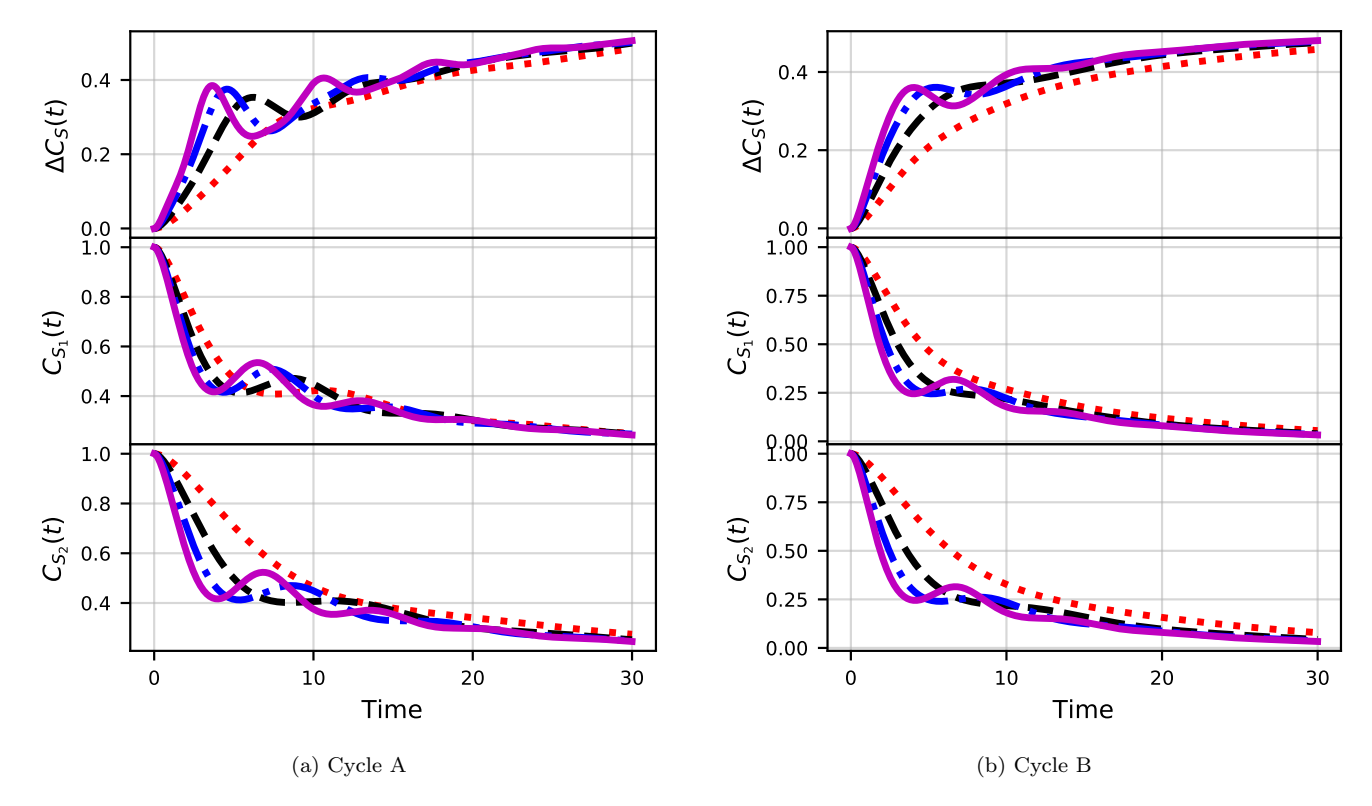


FIG. 8. Local coherences $C_{S_1}(t)$, $C_{S_2}(t)$ and coherence correlation $\Delta C_S(t)$ in the external system. (a) Cycle A: non-monotonic decay of local coherences with persistent and high coherence correlation. (b) Cycle B: faster decay of local coherences and lower coherence correlation, consistent with weaker non-Markovianity. The coupling strength is varied as g = 0.03, 0.05, 0.07, and 0.09 (in units of E_{M_2}), represented by red (dotted), black (dashed), blue (dot-dashed), and magenta (solid) curves.

ACKNOWLEDGMENTS

DATA AVAILABILITY STATEMENT

A. K acknowledges CNRST-Morocco support for this research within the Program " PhD-ASsociate Scholarship – PASS".

DECLARATION OF INTEREST

The authors declare that they have no conflict of interest.

No data statement is available.

- N. M. Myers, O. Abah, and S. Deffner, "Quantum thermodynamic devices: From theoretical proposals to experimental reality," AVS Quantum Sci. 4, 027101 (2022).
- [2] R. Alicki and R. Kosloff, "Introduction to quantum thermodynamics: History and prospects," in *Thermodynamics in the Quantum Regime: Fundamental Aspects and New Directions*, edited by F. Binder, L. A. Correa, C. Gogolin, J. Anders, and G. Adesso (Springer, Cham, 2019), pp. 1–33.
- [3] J. Millen and A. Xuereb, "Perspective on quantum thermodynamics," New J. Phys. 18, 011002 (2016).
- [4] S. Bhattacharjee and A. Dutta, "Quantum thermal machines and batteries," Eur. Phys. J. B 94, 239 (2021).
- [5] P. P. Hofer, JA. B. Brask, M. Perarnau-Llobet, and N. Brunner, "Quantum thermal machine as a thermometer," Phys. Rev. Lett. 119, 090603 (2017).
- [6] R. S. Watson and K. Kheruntsyan, "Quantum manybody thermal machines enabled by atom-atom correlations," SciPost Phys. 18, 190 (2025).
- [7] S. Khandelwal, B. Annby-Andersson, G. F. Diotallevi, A. Wacker, and A. Tavakoli, "Maximal steady-state entanglement in autonomous quantum thermal machines,"

- npj Quantum Inf. 11, 28 (2025).
- [8] J. B. Brask, G. Haack, N. Brunner, and M. Huber, "Autonomous quantum thermal machine for generating steady-state entanglement," New J. Phys. 17, 113029 (2015).
- [9] G. F. Diotallevi, B. Annby-Andersson, P. Samuelsson, A. Tavakoli, and P. Bakhshinezhad, "Steady-state entanglement production in a quantum thermal machine with continuous feedback control," New J. Phys. 26, 053005 (2024).
- [10] M. Aguilar, N. Freitas, and J. P. Paz, "Entanglement generation in quantum thermal machines," *Phys. Rev. A* 102, 062422 (2020).
- [11] R. Silva, G. Manzano, P. Skrzypczyk, and N. Brunner, "Performance of autonomous quantum thermal machines: Hilbert space dimension as a thermodynamical resource," *Phys. Rev. E* 94, 032120 (2016).
- [12] N. Linden, S. Popescu, and P. Skrzypczyk, "How small can thermal machines be? The smallest possible refrigerator," *Phys. Rev. Lett.* 105, 130401 (2010).
- [13] N. Brunner, N. Linden, S. Popescu, and P. Skrzypczyk, "Virtual qubits, virtual temperatures, and the foundations of thermodynamics," *Phys. Rev. E* 85, 051117 (2012).
- [14] A. Usui, W. Niedenzu, and M. Huber, "Simplifying the design of multilevel thermal machines using virtual qubits," *Phys. Rev. A* 104, 042224 (2021).
- [15] A. Khoudiri, A. El Allati, Ö. E. Müstecaphoğlu, and K. El Anouz, "Non-Markovianity and a generalized Landauer bound for a minimal quantum autonomous thermal machine with a work qubit," *Phys. Rev. E* 111, 044124 (2025).
- [16] A. E. Allahverdyan and T. M. Nieuwenhuizen, "Break-down of the Landauer bound for information erasure in the quantum regime," Phys. Rev. E 64, 056117 (2001).
- [17] G. Gour, "Resources of the quantum world," arXiv:2402.05474 [quant-ph] (2024).
- [18] E. Chitambar and G. Gour, "Quantum resource theories," Rev. Mod. Phys. 91, 025001 (2019). Y. Zhou, Q. Zhao, X. Yuan, and X. Ma, "Detecting multipartite entanglement structure with minimal resources," npj Quantum Inf. 5, 83 (2019).
- [19] J. Agustí, C. M. Schneider, K. G. Fedorov, S. Filipp, and P. Rabl, "Non-Markovian thermal reservoirs for autonomous entanglement distribution," arXiv:2506.20742 [quant-ph] (2025).
- [20] G. Zambon and G. Adesso, "Quantum processes as thermodynamic resources: the role of non-Markovianity," *Phys. Rev. Lett.* 134, 200401 (2025).
- [21] M. H. Chakour, K. El Anouz, Y. Hassouni, and A. El Allati, "Improving different thermodynamic quantities in non-Markovian regime," *Quantum Inf. Process.* 24, 1 (2025).
- [22] H. Assil, A. El Allati, and G. L. Giorgi, "Entanglement estimation of Werner states with a quantum extreme learning machine," *Phys. Rev. A* 111, 022412 (2025).
- [23] M. T. Naseem and Ö. E. Müstecaphoğlu, "Engineering entanglement between resonators by hot environment,"

- Quantum Sci. Technol. 7, 045012 (2022).
- [24] G. De Chiara and M. Antezza, "Quantum machines powered by correlated baths," *Phys. Rev. Res.* 2, 033315 (2020).
- [25] P. Doyeux, B. Leggio, R. Messina, and M. Antezza, "Quantum thermal machine acting on a many-body quantum system: Role of correlations in thermodynamic tasks," *Phys. Rev. E* 93, 022134 (2016).
- [26] N. Brunner, M. Huber, N. Linden, S. Popescu, R. Silva, and P. Skrzypczyk, "Entanglement enhances cooling in microscopic quantum refrigerators," *Phys. Rev. E* 89, 032115 (2014).
- [27] M. S. Blok and G. T. Landi, "Quantum thermodynamics for quantum computing," Nat. Phys. 21, 187 (2025).
- [28] G. T. Landi and M. Paternostro, "Irreversible entropy production: From classical to quantum," Rev. Mod. Phys. 93, 035008 (2021).
- [29] S. Deffner and E. Lutz, "Nonequilibrium entropy production for open quantum systems," Phys. Rev. Lett. 107, 140404 (2011).
- [30] M. Popovic, B. Vacchini, and S. Campbell, "Entropy production and correlations in a controlled non-Markovian setting," *Phys. Rev. A* 98, 012130 (2018).
- [31] H. P. Breuer, E. M. Laine, and J. Piilo, "Measure for the degree of non-Markovian behavior of quantum processes in open systems," *Phys. Rev. Lett.* 103, 210401 (2009).
- [32] G. De Tomasi, S. Bera, J. H. Bardarson, and F. Poll-mann, "Quantum mutual information as a probe for many-body localization," *Phys. Rev. Lett.* 118, 016804 (2017).
- [33] X. Meng, J. Gao, and S. Havlin, "Concurrence percolation in quantum networks," *Phys. Rev. Lett.* 126, 170501 (2021).
- [34] S. Chin, "Generalized coherence concurrence and path distinguishability," J. Phys. A: Math. Theor. 50, 475302 (2017).
- [35] D. Mondal, T. Pramanik, and A. K. Pati, "Nonlocal advantage of quantum coherence," *Phys. Rev. A* 95, 010301(R) (2017).
- [36] M. Grajcar, A. Izmalkov, S. H. W. Van der Ploeg, S. Linzen, T. Plecenik, T. Wagner, and A. M. Zagoskin, "Four-qubit device with mixed couplings," *Phys. Rev. Lett.* 96, 047006 (2006).
- [37] M. A. Aamir, P. Jamet Suria, J. A. Marín Guzmán, C. Castillo-Moreno, J. M. Epstein, N. Yunger Halpern, and S. Gasparinetti, "Thermally driven quantum refrigerator autonomously resets a superconducting qubit," Nat. Phys. 21, 318 (2025).
- [38] P. A. Erdman and F. Noé, "Identifying optimal cycles in quantum thermal machines with reinforcement-learning," npj Quantum Inf. 8, 1 (2022).
- [39] A. Rivas, S. F. Huelga, "Open Quantum Systems", Vol. 10, pp. 978–3, Berlin: Springer (2012).
- [40] H. P. Breuer, F. Petruccione, "The Theory of Open Quantum Systems". Oxford: OUP Oxford (2002).